

On the relative influence of the hydrodynamics of lab-scale set-ups and the membrane materials on the rejection of homogeneous metal catalysts in solvent resistant nanofiltration

Antoine Lejeune, Murielle Rabiller-Baudry, Ivo F. J. Vankelecom, Thierry Renouard

▶ **To cite this version:**

Antoine Lejeune, Murielle Rabiller-Baudry, Ivo F. J. Vankelecom, Thierry Renouard. On the relative influence of the hydrodynamics of lab-scale set-ups and the membrane materials on the rejection of homogeneous metal catalysts in solvent resistant nanofiltration. Separation Science and Technology, 2021, 56 (4), pp.766-778. 10.1080/01496395.2019.1706573 . hal-02438535

HAL Id: hal-02438535

https://univ-rennes.hal.science/hal-02438535

Submitted on 13 Feb 2020

HAL is a multi-disciplinary open access archive for the deposit and dissemination of scientific research documents, whether they are published or not. The documents may come from teaching and research institutions in France or abroad, or from public or private research centers.

L'archive ouverte pluridisciplinaire **HAL**, est destinée au dépôt et à la diffusion de documents scientifiques de niveau recherche, publiés ou non, émanant des établissements d'enseignement et de recherche français ou étrangers, des laboratoires publics ou privés.

On the relative influence of the hydrodynamics of lab-scale set-ups and the membrane materials on the rejection of homogeneous metal catalysts in solvent resistant nanofiltration

A. Lejeune[1], M. Rabiller-Baudry[1], I.F.J. Vankelecom[2], T. Renouard[1*]

[1] *Univ Rennes, CNRS, ISCR (Institut des Sciences Chimiques de Rennes) – UMR 6226, F-35000 Rennes, France*

[2] *Membrane Technology Group - cMACS, Faculteit Bio-ingenieurswetenschappen, KU Leuven, B-3001 Leuven, Belgium*

Corresponding author: Dr. Thierry Renouard
Univ Rennes, CNRS, ISCR (Institut des Sciences Chimiques de Rennes) – UMR 6226, 263 avenue du Général Leclerc, F-35000 Rennes, France
thierry.renouard@univ-rennes1.fr

Accepted Manuscript

On the relative influence of the hydrodynamics of lab-scale set-ups and the membrane materials on the rejection of homogeneous metal catalysts in solvent resistant nanofiltration

Solvent resistant nanofiltration is a promising process for homogeneous metal catalyst recovery. However, catalyst rejections are determined using various set-ups with different hydrodynamics, which questions the comparison of the results. The analysis of the membrane performance is another issue even when comparing membranes made of the same material. This study compares the hydrodynamics of three experimental set-ups. Rejections from 57.8 to 80.8% between cross-flow and dead-end SRNF are observed with a Rh catalyst (MW = 258 $g \cdot mol^{-1}$) in toluene. A high throughput screening system is used to analyze the performance of a set of membranes in terms of permeate fluxes and catalyst rejections.

Keywords: Solvent resistant nanofiltration; hydrodynamics; cross-flow; dead-end; homogeneous metal catalyst rejection

Introduction

Production of fine chemicals suffers from difficult separation of multicomponent post-reaction mixtures. In fact, the usual purification steps have many drawbacks because they can be energy-consuming (distillation), need phase change (distillation, crystallization) or consume large amounts of solvents (liquid-liquid extraction). Solvent resistant nanofiltration (SRNF) is a promising separation process **(1-4)** since it can be performed at low temperature, in liquid phase only and without any solvent addition. This makes SRNF an eco-friendly process, favorable to maintain the integrity of fragile molecules. In that sense, SRNF has a huge potential in the field of homogeneous metal catalyst recycling because thermal separation processes can be responsible for their degradation **(5)**. Many papers focus on the recycling of homogeneous and pseudo-homogeneous catalysts by SRNF **(6-14)**. Different strategies are used to improve their

Accepted Manuscript

separation from the final mixture. Variations of membranes **(10,11)**, solvents **(15,16)** and operating conditions (mainly transmembrane pressure **(16,17)** and sometimes temperature **(10)**) are studied as the most important process design parameters.

All these experimental results have been obtained with different lab equipment exhibiting different hydrodynamics **(10,16,18,19)** and the question of their comparison and their transposition to larger flat membranes or industrial spiral-wound modules is open, since fluxes and rejections can vary from one set-up to another **(20)**. Some studies report on the effect of hydrodynamics on membrane performances in aqueous systems **(21-25)** highlighting (i) the positive effect of cross-flow systems to decrease concentration polarization compared to dead-end filtration **(21)** and (ii) the influence of the module scale on the mass transfer for cross-flow **(22-24)** and dead-end filtration **(25)**. However, few studies focus on the influence of hydrodynamic conditions and the scalability of the results in SRNF. Tsibranska and Tylkowsky **(26)** compared fluxes and rejections of phenolics and flavoids with Duramem 300 and 500 membranes in ethanol with a cross-flow set-up (*ca*. 100% rejection) and a stirred dead-end set-up (70-100% rejection). Patterson *et al*. **(27)** also compared cross-flow and dead-end set-ups with the Starmem 122 membrane in toluene. The filtrated trialkylamine bases had lower rejections in cross-flow mode, which was explained by differences in concentration polarization and fouling between the 2 operating modes, even though for one solute the rejection was 19% in dead-end mode and more than 80% in cross-flow SRNF. Shi *et al.* **(28,29)** studied the hydrodynamics of industrial SRNF modules with the PuraMem S600 membrane. Using data from a 1.8”x12” spiral-wound module tested with solutions of sucrose octaacetate in ethyl acetate, correlations were determined to characterize the fluid dynamics as well as the mass transfer coefficient. The solution-diffusion model and the film theory were also used to successfully predict the performances of the

Accepted Manuscript

module of larger size. In addition to the influence of the hydrodynamics, it has to be mentioned that the variance in data is also important since it can affect the ultimate separation process **(30)**.

This paper deals with the comparison of the performances of 3 lab-scale set-ups. Two of them are cross-flow systems and the third one allows dead-end nanofiltration. Their hydrodynamics are first compared using Reynolds numbers and the cross-flow velocity. Then, the toluene fluxes and the rejections of homogeneous metal catalysts obtained with these 3 set-ups are compared to determine the influence of the hydrodynamic conditions. Finally, a dead-end set-up allowing fast membrane screening is used to discuss the effects of solvent and membrane on the catalyst rejection.

Materials and methods

Solvents and metal catalysts

Toluene of analytical grade (>99.3% purity) was provided by Sigma-Aldrich and dimethyl carbonate (DMC, >99% purity) was purchased from Alfa Aesar. The Grubbs-Hoveyda II (**Fig. 1-a**) and $Rh(acac)(CO)_2$ (**Fig. 1-b**) catalysts were provided by Sigma-Aldrich. The properties of the solvents and the metal catalysts are summarized in **Table 1**.

[**Figure 1**]

[**Table 1**]

UV-Vis spectra in toluene and in DMC were recorded in the 280-800 nm range with a Jasco V-630 spectrophotometer equipped with a quartz tube of 1 cm path length. The background was recorded with pure solvent. The concentration of pure Grubbs-Hoveyda II was estimated from its maximum absorbance at λ_{max} = 377 nm and the one of $Rh(acac)(CO)_2$ at λ_{max} = 334 nm using the Beer-Lambert relationship. The accuracy

Accepted Manuscript

of the analyzes was 5%.

Membranes

Various membranes based on polydimethylsiloxane (PDMS) and polyimide (PI) were tested. Their main characteristics are summarized in **Table 2**. Membranes were cut as flat sheet coupons prior to SRNF. For all membranes, one coupon was used for toluene experiments and another one for DMC experiments. The membranes were first compacted in the respective solvent at room temperature under 40 bar pressure until a constant flux was reached. The first milliliters that passed through each membrane sample were discarded because of the possible presence of preservatives. The membrane conditioning can have an impact on its performance **(32)**. For better comparison, the same conditioning was applied to all membranes, even though the Solsep NF070706 was not supposed to be used up to 40 bar (see **Table 2**). It has to be noticed that no damage was observed on the Solsep NF070706 surface after use and several papers already reported on its use under 35-40 bar pressure **(33,34)**.

[**Table 2**]

Filtration conditions and experimental set-ups

For all SRNF experiments, the Grubbs-Hoveyda II initial concentration was 0.5 mM and that of $Rh(acac)(CO)_2$ was 0.05 mM, which corresponds to what can be encountered in catalytic reactions. All nanofiltration experiments were operated at room temperature and at TMP=30 bar, unless otherwise specified, with a volume reduction ratio (VRR) up

Accepted Manuscript

to 2. For all experimental set-ups, sealing was obtained with Viton® O-rings. Wetted rings were FEP-coated to prevent any damage due to the organic solvents.

Cross-flow SRNF with the MET set-up

Flat sheet membranes (17 cm^2) were inserted in circular cells on a commercial stainless steel filtration unit (MET-Evonik, UK) (**Fig. 2**). Two cells were connected in series to make the retentate of the first cell to feed the second one. The cross-flow mode was obtained thanks to a recirculation pump (part of the MET set-up) allowing a flowrate of 1.24 $L \cdot min^{-1}$. Since this feed flowrate was high compared to the permeate flux, an equivalent feed was considered for both membranes. The height of the feed channel was 5 mm. The pressure was obtained thanks to nitrogen pressure applied on the feed tank.

[**Figure 2**]

Cross-flow SRNF with the SEPA cell

A SEPA cell for flat sheet membranes (139 cm^2) was used (**Fig. 3**). The pressure was imposed thanks to a HPLC pump (AZURA P 4.1S, Knauer, Germany) allowing a feed flowrate up to 50 $mL \cdot min^{-1}$. The cross-flow mode was obtained thanks to a recirculation pump allowing a flowrate of 1.24 $L \cdot min^{-1}$. A spacer (**Fig. 4**) was inserted in the retentate compartment in order to promote turbulence (65 mil - thickness of 1.65 mm, Sterlitech, US) as in a spiral module. Without spacer, the height of the feed channel was 2 mm.

[**Figure 3**]

[**Figure 4**]

Dead-end SRNF with the HT-system

Dead-end filtrations were carried out in 2 different high-throughput (HT) filtration

Accepted Manuscript

modules (HTML, Belgium) **(37,38)** called HT-system, allowing for simultaneous filtrations with 6 or 16 membrane samples under the same operating conditions (**Fig. 5**). The 16 positions set-up was used for all experiments in toluene and for some measurements in DMC, while the 6 positions set-up was used for all other DMC experiments (solvent flux and SRNF of solutes). Membrane samples were supported by a porous stainless steel disc. The active area of each membrane sample was 4.52 cm^2 for the 6 positions set-up and 1.54 cm^2 for the 16 positions set-up. The pressure was obtained thanks to nitrogen pressure applied on the feed tank. Feeds were stirred magnetically at 320 rpm (length of the stirrer: 8 cm). Inventors of the system have already checked that all positions were equivalent dealing with fluxes and rejections of rose Bengal in 2-propanol **(37)**, but the system was not characterized yet with respect to hydrodynamics.

[**Figure 5**]

Hydrodynamics

In order to compare the performances of the different set-ups, they were first characterized by their hydrodynamics. The Reynolds number Re is an easy and commonly used way to compare hydrodynamic conditions. It is also often used in correlation to determine the mass transfer coefficient **(39)**. For sake of simplicity, a uniform flow distribution has been assumed above the permeating area of the membranes, even if this assumption does not always correspond with reality **(40,41)**.

Cross-flow SRNF

For a cross-flow nanofiltration, the Reynolds number was calculated according to equation (1). It has to be underlined that for a flow channel (MET set-up, SEPA cell), turbulent conditions start at $Re_{CF} > 2{,}000$.

Accepted Manuscript

$$Re_{CF} = \frac{\rho \times d_H \times u}{\eta} \quad (1)$$

with ρ the solution density ($kg \cdot m^{-3}$), d_H the hydraulic diameter of the liquid flow (m), u the free liquid velocity ($m \cdot s^{-1}$) and η the solution viscosity (Pa·s). Since the solutions were diluted, toluene density and viscosity data were used. d_H and u had to be determined according to some assumptions.

The hydraulic diameter was calculated with equation (2) **(39,42)**.

$$d_H = \frac{2 \times L \times H}{L+H} \quad (2)$$

with L the length of the channel (m) and H the height of the channel (m).

The feed flowrate Q ($m^3 \cdot s^{-1}$) was imposed by a pump and the liquid velocity u ($m \cdot s^{-1}$) in the membrane cell was calculated as follows:

$$u = \frac{Q}{S} \quad (3)$$

Rectangular cell. **Fig. 6** is a layout of the rectangular SEPA cell. The Reynolds number for the SEPA cell was calculated considering a free liquid channel without spacer. It was assumed that the feed passed through the whole length L at the membrane cell entrance. For such a configuration, the flow section S was calculated with equation (4).

$$S = L \times H \quad (4)$$

[**Figure 6**]

Circular cell. For the circular cells of the MET set-up, Reynolds calculations were done considering that the liquid moved as a whirlwind, as illustrated in **Fig. 7**.

[**Figure 7**]

Accepted Manuscript

The length of the flow section was assumed to be the diameter of the pipe where the liquid came from (d=2 mm). The flow section S was calculated with equation 5.

$$S = d \times H \quad (5)$$

Dead-end SRNF

For a dead-end circular cell, the Reynolds number was calculated thanks to equation 6 **(43)**. For a stirred cell (such as the HT-system), a turbulent flow starts at $Re_{DE} > 2 \cdot 10^5$ **(44)**.

$$Re_{DE} = \frac{\rho \times D_{stirrer}{}^2 \times w}{\eta} \quad (6)$$

with $D_{stirrer}$ the diameter of the stirrer (m) and w the angular speed ($rad \cdot s^{-1}$).

SRNF experiments

The same procedure was applied for each experiment whatever the experimental set-up. All nanofiltrations were performed at room temperature (27 ± 4 °C). The first step was to measure the pure solvent flux J_0 ($L \cdot m^{-2} \cdot h^{-1}$) at the desired transmembrane pressure (TMP) using equation 7.

$$J_0 = \frac{V_p}{A \times t} \quad (7)$$

with V_p the volume of permeate (L) recovered during t time (h) and A the membrane filtering area (m^2).

The membrane permeance L_{P_0} ($L \cdot m^{-2} \cdot h^{-1} \cdot bar^{-1}$) was also determined thanks to Darcy's law:

$$J_0 = L_{P_0} \times TMP \quad (8)$$

Accepted Manuscript

Then the solution to filtrate was prepared at the initial concentration (0.05 mM for $Rh(acac)(CO)_2$ and 0.5 mM for Grubbs-Hoveyda II) and the set-up was filled (200 mL of solution for the MET set-up and the HT-system and 260 mL for the SEPA cell). The filtration was performed up to a volume reduction ratio (VRR) equal to 2 (*i.e.* half of the initial feed volume passed through the membrane, equation 9).

$$VRR = \frac{V_{initial\ feed}}{V_{final\ feed}} \quad (9)$$

with $V_{initial\ feed}$ the initial volume of the mixture in the feed tank (L) and $V_{final\ feed}$ the final volume of the mixture in the feed tank (L).

Permeate samples were taken during the filtration in order to measure the permeate flux (J_{SRNF}) and the solute concentration. The final retentate was also analyzed in order to calculate the rejection at VRR=2 using equation (10).

$$Rejection_{VRR=2}\ (\%) = \left(1 - \frac{C_P}{C_R}\right) \times 100 \quad (10)$$

with C_P the concentration of the last permeate sample ($mol \cdot L^{-1}$) and C_R the final retentate concentration ($mol \cdot L^{-1}$).

The remaining solution was then taken off and the set-up was thoroughly rinsed with solvent. Lastly, the pure solvent flux after rinsing (J_R) was measured in order to be compared with the initial solvent flux. For each experiment, the flux measurements (J_0, J_{SRNF}, J_R) were repeated twice and the accuracy was 2%.

Results and discussion

Hydrodynamics of the 3 lab-scale set-ups

The fluid velocities and the Reynolds numbers were calculated for all set-ups (**Table 3**). For the MET set-up, according to **Fig. 7**, the flow was supposed to behave as a

Accepted Manuscript

whirlwind and so a turbulent regime was operated. Cortés-Juan *et al*. **(45)** used Computational Fluid Dynamics to highlight that the flow was partly tangential to the cell wall for a circular cell even if the feed arrived straight inside the cell. Dzhonova-Atanasova *et al*. **(46)** also considered a tangential orientation of the feed pipe resulting in a swirling flow in the cell for a lab-scale set-up (from MET society) with the same geometry as the MET set-up but with an active membrane area of 54 cm². They performed Computational Fluid Dynamics simulations considering a pure water solution and found that the speed of the solution was in the range 0.3-0.9 $m \cdot s^{-1}$ for a feed flowrate of 1.2 $L \cdot min^{-1}$. In these conditions, the Reynolds number was estimated to 8,500. All these data are in accordance with our results.

The SEPA cell seemed to work in laminar conditions (Reynolds < 2,000) but the calculation was performed considering a free liquid channel. It must be underlined that this apparent laminar regime was probably not encountered in the cell because a retentate spacer was added to promote turbulence **(40,47)**. The fluid velocity in the SEPA cell was estimated to 0.13 $m \cdot s^{-1}$. It's noteworthy that in industrial membrane spiral-wound modules, the fluid velocity in a free liquid channel can be estimated by simple assumptions **(48)** and usually ranges from 0.1 to 0.6 $m \cdot s^{-1}$ **(49)** and sometimes reaches 2 $m \cdot s^{-1}$ **(50)**.

The HT-system was developed to work in turbulent conditions, which is highlighted by a high Reynolds number (> 300,000), but it is commonly accepted that dead-end filtrations can increase concentration polarization. Moreover, the calculated Reynolds number is an average value and the local variations along the stirred cell were not taken into account. Actually, the mass transfer decreased continuously with the distance from the sidewall, to reach zero at the center of the set-up **(21,25)**.

[**Table 3**]

Accepted Manuscript

Comparison of the performances in toluene for the 3 set-ups

The previous flow characterization has outlined that different hydrodynamics were encountered with 3 different lab set-ups, thus the influence of hydrodynamics on SRNF results has to be determined. The reported results were calculated using data obtained at final VRR=2, but it has been checked that both flux and rejection were constant throughout the experiments (**Appendix 1**).

Pure toluene fluxes

First, the toluene fluxes of the Sulzer Pervap 4060 (PDMS) and the Starmem 122 (polyimide) membranes were measured with all set-ups, each time using a new membrane coupon (**Fig. 8**). For the SEPA cell, the experiments were performed only with Sulzer Pervap 4060.

For the 3 set-ups, similar toluene fluxes were obtained with Sulzer Pervap 4060 in the 10-30 bar range. For the MET set-up and the SEPA cell, fluxes were so close that they needed to be differently colored to be distinguished in **Fig. 8**. The same trend was also observed with Starmem 122 in the MET set-up and the HT-system. One can guess that the same flux would have been found with the SEPA cell. These results were expected since the solvent flux is known to be independent of the hydrodynamics when the permeate flux is small compared to the feed flow. It can be noticed that the PDMS membrane fluxes were systematically five-fold those measured with the polyimide membrane.

[**Figure 8**]

Fluxes of model solutions

Fluxes during SRNF at TMP=30 bar of the Grubbs-Hoveyda II and $Rh(acac)(CO)_2$ catalysts in toluene (J_{SRNF}) were compared to the pure solvent flux (J_0) at the same

Accepted Manuscript

pressure, for both membranes. **Table 4** gives the J_{SRNF}/J_0 ratios.

For SRNF of Grubbs-Hoveyda II in the HT-system with Starmem 122, the flux with the catalyst was 10% lower than the pure solvent flux (the membrane recovered its initial flux after rinsing) which revealed that concentration polarization occurred in spite of turbulent conditions. Rabiller-Baudry *et al*. **(18)** obtained a more pronounced effect at the same concentration during dead-end SRNF experiments using an apparatus operating under laminar conditions. Actually, they observed that only 35% of the initial flux was maintained, this flux reduction being fully reversible. By changing either the set-up (MET set-up with Starmem 122) or the membrane (HT-system with Sulzer Pervap 4060), the J_{SRNF}/J_0 ratio was close to 1. An additional experiment was realized with the MET cell and the SEPA cell mounted in series (analogous to the replacement of membrane 2 by the SEPA cell in **Fig. 2**) so that both cells were studied exactly under the same operational conditions. Similar J_{SRNF}/J_0 ratios were obtained, thus the influence of the hydrodynamics was limited with these diluted solutions.

For SRNF of $Rh(acac)(CO)_2$, the J_{SRNF}/J_0 ratio was close to 1 for all experiments, meaning that there was no flux decrease. So no concentration polarization can be evidenced through the flux data. This result was expected because the concentration of this catalyst was very small and its effect on the flux was negligible. Nevertheless, an approach combining the film theory and the solution-diffusion model developed by Murthy and Gupta **(51)** can be used to evaluate the solute concentration at the membrane. If the membrane concentration over the bulk concentration ratio (C_m/C_{bulk}) is higher than 1 then concentration polarization occurs. Experimental data obtained with the MET set-up at a TMP of 10 and 30 bar during SRNF of $Rh(acac)(CO)_2$ were used for the calculations (**Table 5**). No concentration polarization was detected with Sulzer Pervap 4060, although concentration polarization was

Accepted Manuscript

evidenced with Starmem 122, even if this was not observed with flux measurements. In the tested 10-30 bar pressure range, the higher the transmembrane pressure, the more significant was the concentration polarization in agreement with the results of Imbrogno and Schäfer **(21)** in water systems. The results obtained with both catalysts emphasize that not only hydrodynamics but also subtle interactions between the solute and the membrane play a major role in SRNF performances.

[**Table 4**]

[**Table 5**]

Rejections of solutes

The rejections of the Grubbs-Hoveyda II and the $Rh(acac)(CO)_2$ catalysts at TMP=30 bar were then compared with the 3 set-ups, using both membranes (**Table 4**). As a general trend, the rejections obtained with Starmem 122 were higher than those obtained with Sulzer Pervap 4060. This can be put in parallel to the much lower fluxes of the former membrane.

The rejection of the Grubbs-Hoveyda II catalyst with Starmem 122 was the same with the MET set-up and the HT-system (99.6%). Both cross-flow set-ups also revealed similar catalyst rejections with Sulzer Pervap 4060 (*ca*. 95% at TMP=10 bar). For that experiment, the slightly lower rejection can be partly attributed to the lower pressure applied during SRNF. For a strongly retained solute, it seemed that the cross-flow or dead-end hydrodynamics had no impact on the rejection.

The rejection of $Rh(acac)(CO)_2$ varied from 35% to 81%, depending on the set-up or the membrane used. Similar to what was observed with the Grubbs-Hoveyda II catalyst, both cross-flow set-ups exhibited comparable rejections. However, the rejection was at least 20 percent higher with the HT-system (dead-end mode) whatever

Accepted Manuscript

the membrane. This can be correlated to the optimized hydrodynamics developed for the HT-system as pointed out by its high Reynolds number.

These preliminary results highlight that the membrane material mainly drives the SRNF performances and that hydrodynamics has a small impact on solvent flux and rejection for very highly retained solutes (for concentrations in the millimolar range) whereas hydrodynamics plays a major role for solutes with intermediate rejections. Hence, in the following, a membrane screening was performed with the HT-system, allowing to study the membranes performances exactly under the same operational conditions and hydrodynamics.

Membrane screening in toluene and DMC with the HT-system

A set of PDMS and polyimide membranes were tested. Their characteristics are summarized in **Table 2**. The filtrated solutions were prepared with the catalyst as a single solute. It has to be noticed that real reaction mixtures would be more complex, since mainly composed of some remaining substrate, the target product and several by-products, in addition to the catalyst residue. The substrate/product concentrations are usually high (up to 1 $mol \cdot L^{-1}$ **(52)**) which may induce a rejection variation due to either interactions between the catalyst and the organic products or modification of the solution viscosity.

Solvent fluxes

Pure solvent fluxes at TMP=30 bar were first measured (**Fig. 9**). Toluene fluxes were measured with the 16 positions HT-system. Fluxes in DMC were measured with the 6 and 16 positions HT-system and proved to be equivalent with both set-ups. The DMC viscosity and density were close to those of toluene (**Table 1**) meaning that the flow remained turbulent in DMC (Re_{DE}=395,283 > 200,000).

Accepted Manuscript

As a general trend, the DMC flux was higher than the toluene flux (which was not measured for the Solsep NF030306F and both Duramem membranes, since they had an extremely low permeance), except for Sulzer Pervap 4060, Solsep NF070706 and Starmem 240 exhibiting a much higher toluene flux. The membrane material was not the only factor influencing the permeance since the 2 PDMS membranes Solsep NF070706 and NF030306 had respectively the highest and the lowest toluene fluxes and the 2 PI membranes Starmem 122 and 240 had respectively the highest and the lowest DMC fluxes. The MWCO is commonly considered as being the main difference between the last 2 PI membranes, but other manufacturing differences (active layer thickness, additives,…) are necessary to tackle their reversed behavior from toluene to DMC.

[**Figure 9**]

Solvent fluxes were also measured during SRNF experiments. In toluene, the J_{SRNF}/J_0 ratio was close to 1 for all membranes during the filtration of all catalysts (Data not shown). This was also true in DMC, except for SRNF of Grubbs-Hoveyda II with the Starmem 240 membrane (J_{SRNF}/J_0=0.56). Keraani *et al*. **(53)** were the first ones to perform SRNF of Grubbs-Hoveyda II in DMC. They used a Starmem 228 membrane in a dead-end set-up and observed a J_{SRNF}/J_0ratio of 0.82 at a TMP of 25 bar.

Catalyst rejections

The Grubbs-Hoveyda II catalyst rejections were first determined (**Fig. 10**). For toluene solutions, the rejection reached 99.6% with Starmem 122 and 90.0% with Sulzer Pervap 4060 but was lower than 65% with all other membranes. The highest rejection was obtained with Starmem 122 which also had the lowest flux, whereas Sulzer Pervap 4060 exhibited one of the highest rejection as well as the highest flux. Thus, a clear

Accepted Manuscript

relationship between toluene flux and catalyst rejection cannot be drawn, as could be expected from membrane permeations where affinity of the solvent or the solute for the membrane also plays a role **(31,54,55)**.

Three membranes were tested for the Grubbs-Hoveyda II rejection in DMC. The maximum rejection was 94.8% with Starmem 240, comparable to the maximum rejection observed with toluene. This should be of importance for productivity reasons since the rejection of the reaction product is an issue quite frequently omitted: the high MWCO of Starmem 240 compared to Starmem 122 should favor the reaction product permeance. For the 2 PDMS Solsep membranes, the rejections were quite different: 53.6% with NF030306 and almost 2.3% with NF070706, thus the highest rejection was obtained with the membrane exhibiting the highest MWCO.

[**Figure 10**]

In toluene, $Rh(acac)(CO)_2$ always had a lower rejection than the Grubbs-Hoveyda II catalyst (**Fig. 10**). This result was expected because of their molecular weight difference. Its rejection was higher than 80% only with Starmem 122.

In the case of DMC solutions, the $Rh(acac)(CO)_2$ rejection was 86% with Solsep NF030306. The 2 other tested membranes had a rejection lower than 30%. It seemed that, in DMC, the PDMS-based membranes from Solsep had a low affinity for $Rh(acac)(CO)_2$ (high rejection) whereas they had a quite good affinity for the Grubbs-Hoveyda II catalyst (low rejection). An opposite trend was observed with the Starmem 240 membrane made of Polyimide.

The results obtained with Solsep NF070706 and Starmem 240 can be used for a global comparison since these 2 membranes were tested with both solvents and both catalysts. Although made of different materials, they exhibited a much higher toluene flux than DMC flux and comparable catalysts rejections that followed the same trend,

Accepted Manuscript

except for the Grubbs-Hoveyda II rejection in DMC. This final point outlines that even though a clear tendency can be observed when comparing the membrane performance, the extrapolation of results is still delicate.

Conclusion

The hydrodynamics of 3 lab-scale set-ups were characterized thanks to simple but realistic assumptions and different flow conditions were revealed. SRNF of two organometallic catalysts was performed with the 3 set-ups, to study to what extent hydrodynamics can affect the filtration results. Rejections varied from 57.8 to 80.8% between cross-flow and dead-end apparatuses for $Rh(acac)(CO)_2$ (rejection), while rejections always remained high for Grubbs-Hoveyda II, whatever the set-up. These results highlight that for solutes of intermediate rejections, the hydrodynamics may play a more important role on the rejection than for highly retained solutes.

The HT-system working in dead-end mode and allowing simultaneous SRNF with several membranes was used for fast membrane screening. Promising combinations (solvent, catalyst and membrane) were found (*e.g.* Starmem 122 gave almost full rejection of Grubbs-Hoveyda II in toluene), but no systematic trend could be withdrawn highlighting that "trial and error" experiments might still be necessary to select an optimal combination. In addition to the time consuming "trial and error" approach, the design of experiments (DoE) analysis could reveal further trends.

Acknowledgements

The authors thank the french ANR (Agence Nationale de la Recherche) for the financial support of the project MemChem n° 14-CE06-0022 and the french clusters IAR and Axelera for labelling this project.

Accepted Manuscript

References

1. Marchetti, P.; Jimenez Solomon, M.; Szekely, G.; Livingston, A. (2014) Molecular Separation with Organic Solvent Nanofiltration: A Critical Review. *Chem. Rev.*, 114 (21): 10735.

2. Buonomenna, M.G.; Bae, J. (2015) Organic Solvent Nanofiltration in Pharmaceutical Industry. *Sep. Purif. Rev.*, 44 (2): 157.

3. Vandezande, P.; Gevers, L.; Vankelecom, I. (2008) Solvent resistant nanofiltration: separating on a molecular level. *Chem. Soc. Rev.*, 37 (2): 365.

4. Vankelecom, I. (2002) Polymeric Membranes in Catalytic Reactors. *Chem. Rev.*, 102 (10): 3779.

5. Csera, L.; Fodi, T.; Kupai, J.; Balogh, G.; Garforth, A.; Szekely, G. (2017) Membrane-assisted catalysis in organic media. *Adv. Mater. Lett.*, 8 (12): 1094.

6. Peeva, L.; Da Silva Burgal, J.; Heckenast, Z.; Brazy, F.; Cazenave, F.; Livingston, A. (2016) Continuous Consecutive Reactions with Inter-Reaction Solvent Exchange by Membrane Separation. *Angew. Chem. Int.*, 55 (43): 13576.

7. Dreimann, J.; Lutze, P.; Zagajewsky, M.; Behr, A.; Górak, A.; Vorholt, A. (2016) Highly integrated reactor–separator systems for the recycling of homogeneous catalysts. *Chem. Eng. Process*, 99: 124.

8. O'Neal, E.; Jensen, K. (2014) Continuous Nanofiltration and Recycle of a Metathesis Catalyst in a Microflow System. *ChemCatChem*, 6 (10): 3004.

9. Siew, W.; Ates, C.; Merschaert, A.; Livingston A. (2013) Efficient and productive asymmetric Michael addition: development of a highly enantioselective quinidine-based organocatalyst for homogeneous recycling via nanofiltration. *Green Chem.*, 15 (3): 663.

10. Cano-Odena, A.; Vandezande, P.; Fournier, D.; Van Camp, W.; Du Prez, F.; Vankelecom, I. (2010) Solvent-resistant nanofiltration for product purification and catalyst recovery in click chemistry reactions. *Chem. Weinh. Bergstr. Ger.*, 16 (3): 1061.

11. Aerts, S.; Buekenhoudt, A.; Weyten, H.; Gevers, L.; Vankelecom, I., Jacobs, P. (2006) The use of solvent resistant nanofiltration in the recycling of the Co-Jacobsen catalyst in the hydrolytic kinetic resolution (HKR) of epoxides. *J. Membr. Sci*., 280 (1-2): 245.

12. Mertens, P.; Bulut, M.; Gevers, L.; Vankelecom, I.; Jacobs, P.; Vos, D. (2005) Catalytic oxidation of 1,2-diols to α-hydroxy-carboxylates with stabilized gold nanocolloids combined with a membrane-based catalyst separation. *Catal. Lett.*, 102 (1-2): 57.

13. Großeheilmann, J.; Büttner, H.; Kohrt, C.; Kragl, U.; Werner, T. (2015) Recycling of phosphorus-based Organocatalysts by Organic Solvent Nanofiltration. *ACS Sustainable Chem. Eng.*, 3: 2817.

14. Kisszekelyi, P.; Alammar, A.; Kupai, J., Huszthy, P.; Barabas, J.; Holtzl, T.; Szente, L.; Bawn, C.; Adams, R.; Szekely, G. (2019) Asymmetric synthesis with cinchona-decorated cyclodextrin in a continuous-flow membrane reactor. *J. Catal.*, 371: 255.

Accepted Manuscript

15. Ormerod, D.; Bongers, B.; Porto-Carrero, W.; Giegas, S.; Vijt, G.; Lefevre, N.; Lauwers, D.; Brusten, W.; Buekenhoudt, A. (2013) Separation of metathesis catalysts and reaction products in flow reactors using organic solvent nanofiltration. *RSC Adv.*, 3 (44): 21501.

16. Razak, N.; Shaharun, M.; Mukhtar, H.; Taha, M. (2013) Separation of hydridocarbonyltris(triphenylphosphine) rhodium (I)catalyst using solvent resistant nanofiltration membrane. *Sains Malays.*, 42 (4): 515.

17. Shaharun, M.; Taha, M. (2012) Nanofiltration of rhodium tris(triphenylphosphine) catalyst in ethyl acetate solution. *American Institute of Physics*, Conference Proceedings.

18. Rabiller-Baudry, M.; Nasser, G.; Renouard, T.; Delaunay, D.; Camus, M. (2013) Comparison of two nanofiltration membrane reactors for a model reaction of olefin metathesis achieved in toluene. *Sep. Purif. Technol.*, 116: 46.

19. Nasser, G.; Renouard, T.; Shahane, S.; Fischmeister, C.; Bruneau, C.; Rabiller-Baudry, M. (2013) Interest of the Precatalyst Design for Olefin Metathesis Operating in a Discontinuous Nanofiltration Membrane Reactor. *ChemPlusChem*, 78 (7): 728.

20. Goebel, R.; Schreiber, M.; Koleva, V.; Horn, M.; Gorak, A.; Skiborowski, M. (2019) On the reliability of lab-scale experiments for the determination of membrane specific flux measurements in organic solvent nanofiltration. *Chem. Eng. Res. Des.*, 148: 271.

21. Imbrogno, A.; Schäfer, A. (2019) Comparative study of nanofiltration membrane characterization devices of different dimension and configuration (cross flow and dead end). *J. Membr. Sci.*, 585: 67.

22. Belfort, G. (1988) Membrane modules: comparison of different configurations using fluid mechanics. *J. Membr. Sci.*, 35 (3): 245.

23. Mavrov, V.; Nikolov, N.; Islam, M.; Nikolova, J. (1992) An investigation on the configuration of inserts in tubular ultrafiltration module to control concentration polarization. *J. Membr. Sci.*, 75 (1-2): 197.

24. Ren, Z.; Yang, Y.; Zhang, W.; Liu, J.; Wang, H. (2013) Modeling study on the mass transfer of hollow fiber renewal liquid membrane: Effect of the hollow fiber module scale. *J. Membr. Sci.*, 439: 28.

25. Zydney, A.; Xenopoulos, A. (2007) Improving dextran tests for ultrafiltration membranes: effect of device format. *J. Membr. Sci.*, 291: 180.

26. Tsibranska, I.; Tylkowsky, B. (2013) Concentration of ethanolic extracts from Sideritis ssp. L. by nanofiltration: Comparison of dead-end and cross-flow modes. *Food Bioprod. Process.*, 91 (2): 169.

27. Patterson, D.; Yen Lau, L.; Roengpithya, C.; Gibbins, E.; Livingston, A. (2008) Membrane selectivity in the organic solvent nanofiltration of trialkylamine bases. *Desalination*, 218 (1-3): 248.

28. Shi, B.; Peshev, D.; Marchetti, P.; Zhang, S.; Livingston, A. (2016) Multi-scale modelling of OSN batch concentration with spiral-wound membrane modules using OSN Designer. *Chem. Eng. Res. Des.*, 109: 385.

Accepted Manuscript

29. Shi, B.; Marchetti, P.; Peshev, D.; Zhang, S.; Livingston, A. (2015) Performance of spiral-wound membrane modules in organic solvent nanofiltration – Fluid dynamics and mass transfer characteristics. *J. Membr. Sci.*, 494: 8.

30. Böcking, A.; Koleva, V.; Wind, J.; Thiermeyer, Y.; Blumenschein, S.; Goebel, R.; Skiborowski, M.; Wessling, M. (2019) Can the variance in membrane performance influence the design of organic solvent nanofiltration processes? *J. Membr. Sci.*, 575: 217.

31. Ben Soltane, H.; Roizard, D.; Favre, E. (2016) Study of the rejection of various solutes in OSN by a composite polydimethylsiloxane membrane: Investigation of the role of solute affinity. *Sep. Purif. Technol*., 161: 193.

32. Razali, M.; Didaskalou, C.; Kim, J.; Babaei, M.; Drioli, E.; Lee, Y-M.: Szekely, G. (2017) Exploring and Exploiting the Effect of Solvent Treatment in Membrane Separations. *ACS Appl. Mater. Interfaces*, 9: 11279.

33. Bastin, M.; Hendrix, K.; Vankelecom, I. (2017) Solvent resistant nanofiltration for acetonitrile based feeds: A membrane screening. *J. Memb. Sci.*, 536: 176.

34. Teixeira, A.; Santos, J.; Crespo, J. (2014) Assessment of solvent resistant nanofiltration membranes for valorization of deodorizer distillates. *J. Memb. Sci.*, 470: 138.

35. Zeidler, S.; Kätzel, U.; Kreis, P. (2013) Systematic investigation on the influence of solutes on the separation behavior of a PDMS membrane in organic solvent nanofiltration. *J. Membr. Sci.*, 429: 295.

36. Soroko, I.; Lopes, M.; Livingston, A. (2011) The effect of membrane formation parameters on performance of polyimide membranes for organic solvent nanofiltration (OSN): Part A. Effect of polymer/solvent/non-solvent system choice. *J. Membr. Sci.*, 381 (1-2): 152.

37. Vandezande, P.; Gevers, L.; Paul, J.; Vankelecom, I.; Jacobs, P. (2005) High throughput screening for rapid development of membranes and membrane processes. *J. Membr. Sci.*, 250 (1-2): 305.

38. High Throughput Membrane systems - Leuven, http://www.biw.kuleuven.be/cok/membrane2/ (accessed in November, 2019).

39. Wang, J.; Dlamini, D.; Mishra, A.; Pendergast, M.; Wong, M.; Mamba, B.; Freger, V.; Verliefde, A.; Hoek, E. (2014) A critical review of transport through osmotic membranes. *J. Membr. Sci.*, 454: 516.

40. Delaunay, D.; Rabiller-Baudry, M; Gozálvez-Zafrilla, J.; Balannec, B.; Frappart, M.; Paugam, L. (2008) Mapping of protein fouling by FTIR-ATR as experimental tool to study membrane fouling and fluid velocity profile in various geometries and validation by CFD simulation. *Chem. Eng. Process.*, 47 (7): 1106.

41. Kawachale, N.; Kumar, A.; Kirpalani, D. (2009) A flow distribution study of laboratory scale membrane gas separation cells. *J. Membr. Sci.*, 332 (1-2): 81.

42. Schock, G.; Miquel, A. (1987) Mass transfer and pressure loss in spiral wound modules. *Desalination*, 64: 339.

Accepted Manuscript

43. Becht, N.; Malik, D.; Tarleton, E. (2008) Evaluation and comparison of protein ultrafiltration test results: Dead-end stirred cell compared with a cross-flow system. *Sep. Purif. Technol.*, 62 (1): 228.

44. Randriamampianina, A.; Elena, L.; Fontaine, J.; Schiestel, R. (1997) Numerical prediction of laminar, transitional and turbulent flows in shrouded rotor-stator systems, *Phys. Fluids*, 9 (6): 1696.

45. Cortés-Juan, F.; Balannec, B.; Renouard, T. (2011) CFD-assisted design improvement of a bench-scale nanofiltration cell. *Sep. Purif. Technol.*, 82: 177.

46. Dzhonova-Atanasova, D.; Tsibranska, I.; Vlaev, S. (2017) Flow behaviour in a membrane cross-flow filtration cell: experimental observations and CFD modelling. *J. Chem. Technol. Metal.*, 52 (1): 58.

47. Santos, J.; Geraldes, V.; Velizarov, S.; Crespo, J. (2007) Investigation of flow patterns and mass transfer in membrane module channels filled with flow-aligned spacers using computational fluid dynamics (CFD). *J. Membr. Sci.*, 305 (1-2): 103.

48. Rabiller-Baudry, M.; Diagne, N; Lebordais, D. (2014) How the experimental knowledge of the irreversible fouling distribution can contribute to understand the fluid circulation in a spiral ultrafiltration membrane. *Sep. Purif. Technol.*, 136: 157.

49. Scott, K. (1995) *Handbook of Industrial Membranes*, 1stEd.; Elsevier, The Netherlands.

50. Shaabana, A.; Hazefa, A.; Abdel-Fataha, M.; Abdel-Monemb, N.; Mahmoud, M. (2016) Process engineering optimization of nanofiltration unit for the treatment of textile plant effluent in view of solution diffusion model. *Egyt. J. Petrol.*, 24 (1): 79.

51. Murphy, Z.; Gupta, S. (1997) Estimation of mass transfer coefficient using a combined nonlinear membrane transport and film theory model. *Desalination*, 109 (1): 39.

52. Renouard, T., Lejeune, A., Rabiller-Baudry, M. (2018) Separation of solutes with an organic solvent nanofiltration cascade: Designs, simulations and systematic study of all configurations. *Sep. Purif. Technol.*, 194: 111.

53. Keraani, A.; Renouard, T.; Fischmeister, C.; Bruneau, C.; Rabiller-Baudry, M. (2008) Recovery of enlarged olefin metathesis catalysts by nanofiltration in an eco-friendly solvent. *ChemSusChem*, 1 (11): 927.

54. Verliefde, A.; Cornelissen, E.; Heijman, S.; Hoek, E.; Amy, G.; Van der Bruggen, B.; Van Dijk, J. (2009) Influence of Solute−Membrane Affinity on Rejection of Uncharged Organic Solutes by Nanofiltration Membranes. *Environ. Sci. Technol.*, 43 (7): 2400.

55. Postel, S.; Schneider, C.; Wessling, M. (2016) Solvent dependent solute solubility governs retention in silicone based organic solvent nanofiltration. *J. Membr. Sci.*, 497: 47.

Accepted Manuscript

Table 1. Solvents and solutes properties

Component	Molecular weight ($g \cdot mol^{-1}$)	Density	Viscosity at 25°C (mPa·s)	ε_r	Solubility parameter $(J \cdot cm^{-3})^{0.5}$
Toluene	92	0.867	0.55	2.38	18.2 **(31)**
Dimethyl carbonate	90	1.069	0.58	3.08	20.2 **(31)**
Grubbs-Hoveyda II	627	-	-	-	-
$Rh(acac)(CO)_2$	258	-	-	-	-

Table 2. SRNF membranes characteristics[(a)]

Provider	Reference	Active layer material	MWCO ($g \cdot mol^{-1}$)	T_{max} (°C)	TMP_{max} (bar)	Solubility parameter $(J \cdot cm^{-3})^{0.5}$
Sulzer	Pervap 4060	PDMS	-	-	-	15.5 **(35)**
Solsep	NF030306	PDMS	500	150	40	15.5 **(35)**
Solsep	NF030306F	PDMS	500	150	40	15.5 **(35)**
Solsep	NF070706	PDMS	250	100	20	15.5 **(35)**
MET-Evonik	Duramem 300	PI	300	50	60	23.1 **(36)**
MET-Evonik	Duramem 200	PI	200	50	60	23.1 **(36)**
MET-Evonik	Starmem 122	PI	220	60	60	27.0 **(36)**
MET-Evonik	Starmem 240	PI	400	60	60	27.0 **(36)**

[(a)] Manufacturer data - PDMS : polydimethylsiloxane ; PI : polyimide

Accepted Manuscript

Table 3. Hydrodynamic characteristics of the 3 lab-scale set-ups

	MET set-up	SEPA cell	HT-system
Mode of SRNF	Cross-flow	Cross-flow	Dead-end
d_H (mm) / $D_{stirrer}$ (cm)	3	4	8
u ($m \cdot s^{-1}$) / w (rpm)	2.07	0.13	320
Reynolds number (-)	9308	803	338,076

Table 4. SRNF performances in toluene at TMP=30 bar and VRR=2

Membrane	Set-up	Duration (min)	Grubbs-Hoveyda II Initial concentration=0.5 mM		$Rh(acac)(CO)_2$ Initial concentration=0.05 mM	
			J_{SRNF}/J_0	Rejection (%)	J_{SRNF}/J_0	Rejection (%)
Starmem 122	MET set-up	100	1.05	99.6±7.0	1.01	57.8±4.1
	HT-system	120	0.90	99.6±7.0	1.12	80.8±5.7
Sulzer Pervap 4060	MET set-up	30	0.89[(a)]	95.4±6.7[(a)]	1.05	40.0±2.8
	SEPA cell	30	0.93[(a)]	94.9±6.7[(a)]	1.02	35.1±2.5
	HT-system	50	1.00	90.0±6.4	1.00	60.9±4.3

[(a)] MET and SEPA cells in series, TMP=10 bar

Table 5. Membrane over bulk concentration ratio (C_m/C_{bulk}) of $Rh(acac)(CO)_2$ during SRNF in toluene with the MET set-up (initial concentration=0.05 mM)

	TMP=10 bar	TMP=30 bar
Starmem 122	1.49	3.42
Sulzer Pervap 4060	1.01	1.03

Accepted Manuscript

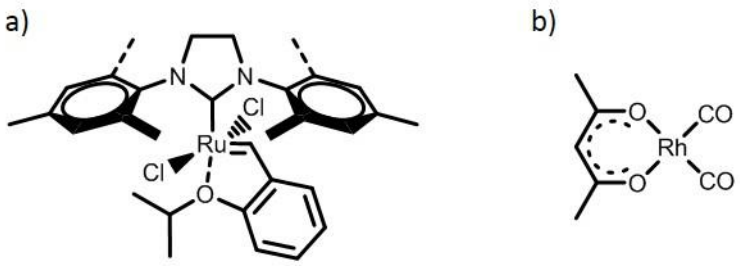


Figure 1. Structure of the catalysts: a) Grubbs-Hoveyda II ; b) $Rh(acac)(CO)_2$

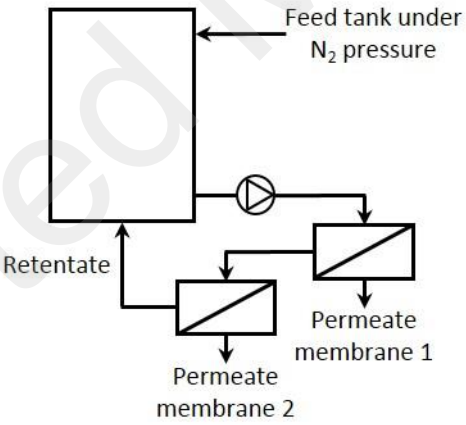


Figure 2. Outline of the MET-Evonik filtration unit

Accepted Manuscript

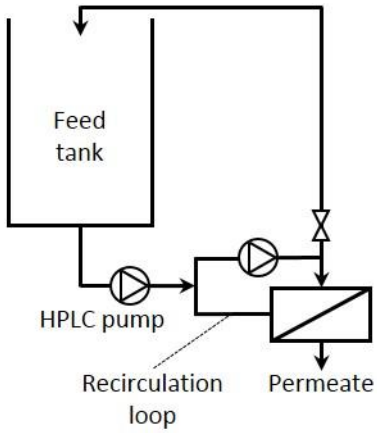


Figure 3. Outline of the SEPA cell set-up

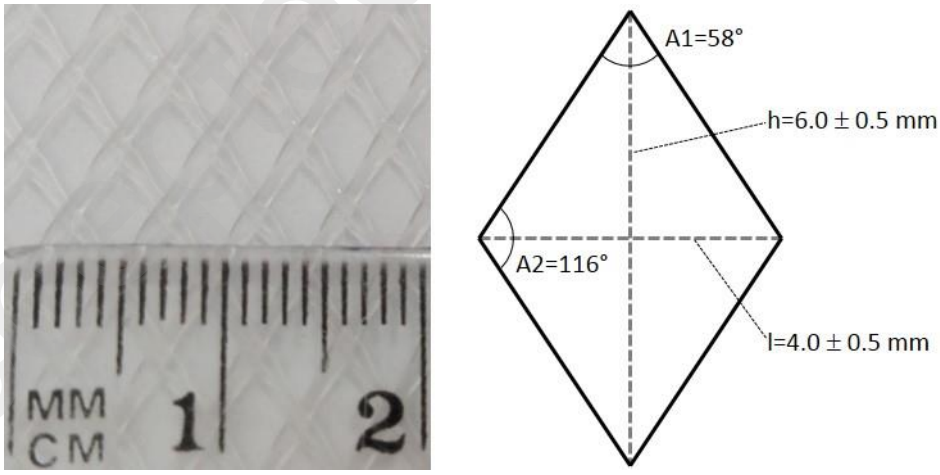


Figure 4. Picture of the spacer used in the SEPA cell (left) and its geometric characteristics (right)

Accepted Manuscript

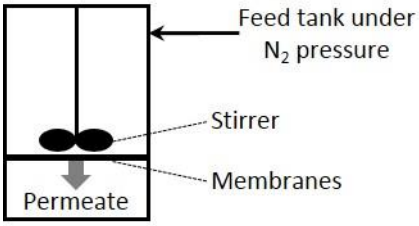


Figure 5. Outline of the HT-system

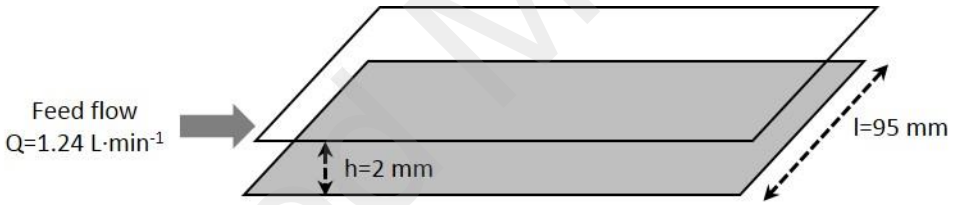


Figure 6. Outline of the inside of the SEPA cell

Accepted Manuscript

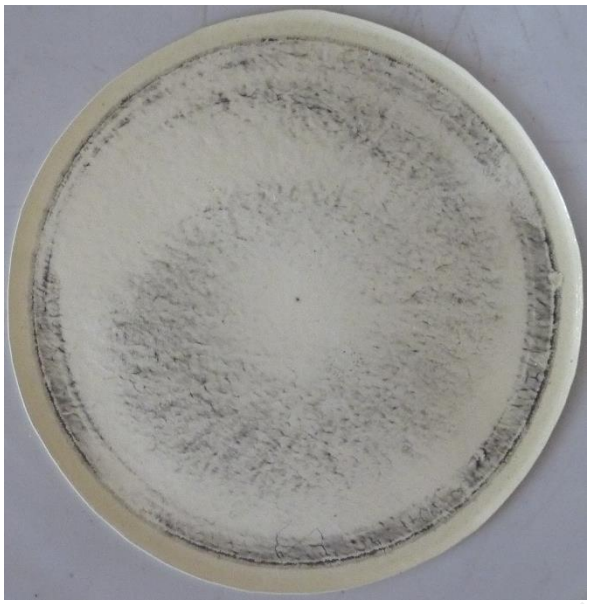


Figure 7. Picture of a membrane coupon after its use with the MET set-up

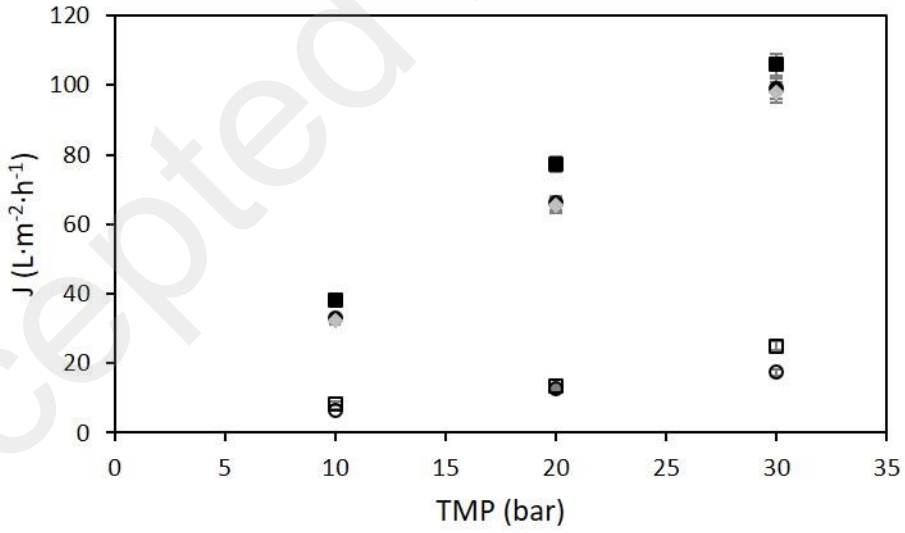


Figure 8. Toluene flux of Sulzer Pervap 4060 (full points) and Starmem 122 (empty points) – ○ : MET set-up ; ◊ : SEPA cell ; □ : HT-system (16 positions)

Accepted Manuscript

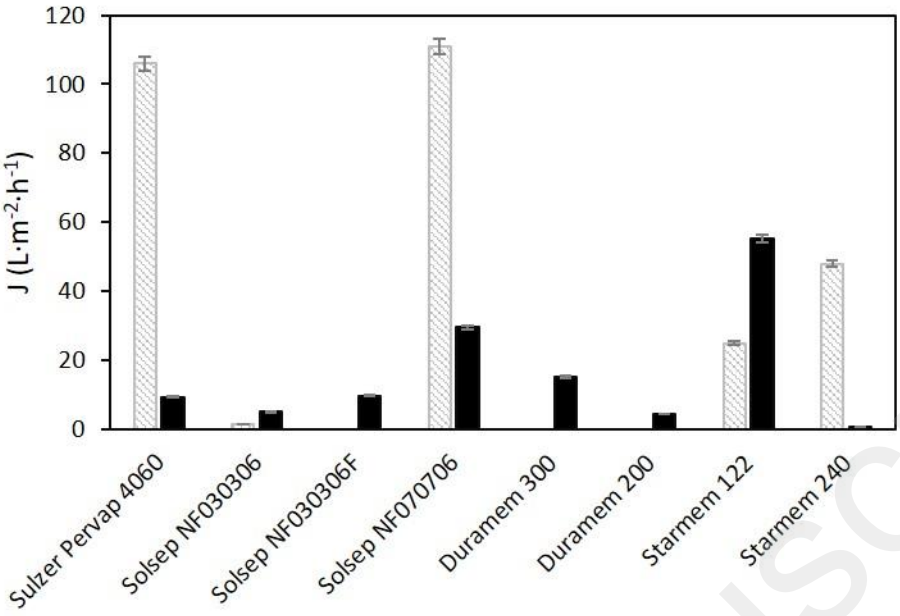


Figure 9. Pure solvent flux at TMP=30 bar with the HT-system - Toluene : dashed column - DMC : full column

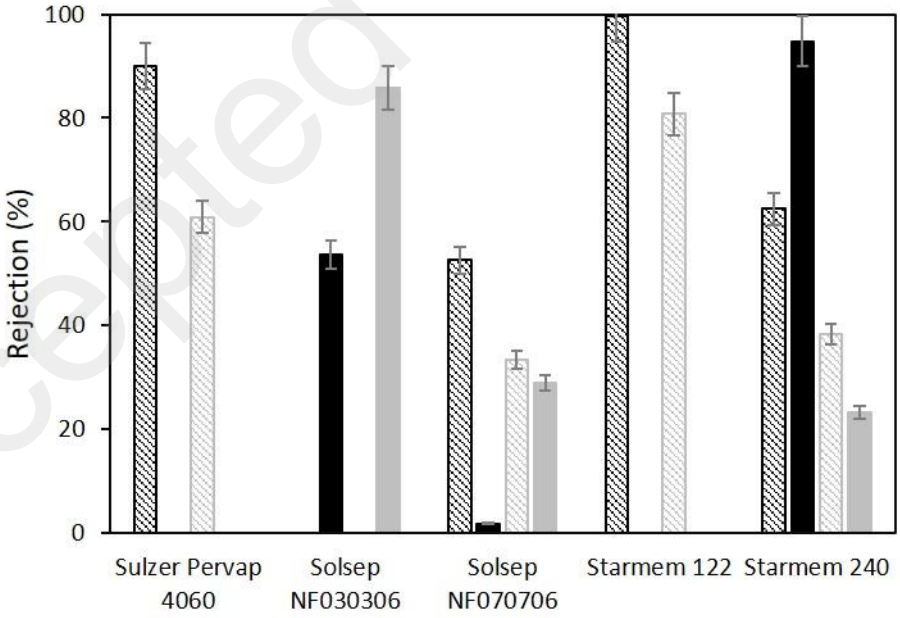


Figure 10. Grubbs-Hoveyda II (black) and $Rh(acac)(CO)_2$ (grey) rejections with the HT-system in toluene (dashed column) and DMC (full column) at TMP=30 bar and VRR=2

Accepted Manuscript

Figure 1. Structure of the catalysts: a) Grubbs-Hoveyda II ; b) $Rh(acac)(CO)_2$

Figure 2. Outline of the MET-Evonik filtration unit

Figure 3. Outline of the SEPA cell set-up

Figure 4. Picture of the spacer used in the SEPA cell (left) and its geometric characteristics (right)

Figure 5. Outline of the HT-system

Figure 6. Outline of the inside of the SEPA cell

Figure 7. Picture of a membrane coupon after its use with the MET set-up

Figure 8. Toluene flux of Sulzer Pervap 4060 (full points) and Starmem 122 (empty points) – ○ : MET set-up ; ◊ : SEPA cell ; □ : HT-system (16 positions)

Figure 9. Pure solvent flux at TMP=30 bar with the HT-system - Toluene : dashed column - DMC : full column

Figure 10. Grubbs-Hoveyda II (black) and $Rh(acac)(CO)_2$ (grey) rejections with the HT-system in Toluene (dashed column) and DMC (full column) at TMP=30 bar and VRR=2

Accepted Manuscript